Author version: *Palaeogeogr. Palaeoclimatol. Palaeoecol., vol.397; 2014; 31-37*

Change in the intensity of low-salinity water inflow from the Bay of Bengal into the Eastern Arabian Sea from the Last Glacial Maximum to the Holocene: Implications for monsoon variations

B. S. Mahesh[1] and V. K. Banakar[*]

CSIR-National Institute of Oceanography, Dona Paula, Goa-403 004, India

1- Present Address: National Centre for Antarctic and Ocean Research, Headland Sada, Vasco-da-Gama, Goa, India

Abstract

A 100-400 km wide region of the coastal Eastern Arabian Sea (EAS), off the west-coast of India, is characterized by a low-salinity tongue formed by the inflow of low-salinity surface water from the Bay of Bengal (BoB). This low-salinity tongue is largely driven by the sea level higher in BoB than in the Arabian Sea and by alongshore pressure gradient between southern- and northern- EAS, and is expected to respond to summer monsoon freshwater flux to the bay. Here, we report past variation in the relative intensity of summer- and winter- monsoons based on changes in the north-south salinity gradient within this low-salinity tongue. The salinity gradient is estimated from paired measurement of $\delta^{18}O$ and Mg/Ca in *Globigerinoides sacculifer* extracted from sediment cores collected at northern high-salinity and southern low-salinity locations within this tongue.

The Last Glacial Maximum (LGM) to peak-Holocene $\delta^{18}O$ and sea surface temperature gradients at both locations are ~ −2 ‰ and +2^{o}C respectively, while the sea surface salinity gradient at northern-EAS is 0.5 psu higher than in the southern-EAS, suggesting distinctly different SSS structure in the LGM-EAS. The north-south surface salinity gradient was also larger by ~0.5 psu during the LGM (1.2 psu) as compared to the gradient during the Holocene (0.7 psu). Increased north-south surface salinity gradient during the LGM suggests diminished flow of low-salinity water into the coastal EAS caused by combined effect of decreased freshening of the BoB and reduced seasonal mountain-rivers discharge into the EAS. Such surface hydrographic conditions in the coastal EAS clearly indicate significantly weakened summer monsoons and strengthened winter monsoons during the LGM.

Key Words: Arabian Sea, Indian monsoon, paleo-SST, paleo-salinity, Planktonic foraminifera $\delta^{18}O$ and Mg/Ca

**Corresponding author: e-mail: banakar@nio.org*

Introduction

The sea surface- temperature (SST) and -salinity (SSS) in the Eastern Arabian Sea (EAS) are readily influenced by the strength of seasonally reversing monsoons, characteristic of the northern Indian Ocean. The monsoon dynamics also drive the inter-basin exchange of surface water between perennially less-saline Bay of Bengal (BoB) and more-saline Arabian Sea (Shetye et al., 1991; Shankar and Shetye, 2001). Evaporation dominant (E-P > 1) conditions in the Arabian Sea, and precipitation dominant (E-P < 1) conditions in the BoB, together result in distinctly different SSS structure between these two basins (Prasanna Kumar and Prasad, 1999; Wilson et al., 2009). The contrasting E-P along with local wind forcing during the post-summer monsoon period cause differing sea levels between the southeast- and southwest- coasts of India, which result in alongshore pressure gradient, forcing the low-salinity BoB water to flow into the EAS (Shankar and Shetye, 2001). Model runs have been able to reproduce this climatological set-up, driving the low-salinity water plume entering into the EAS from BoB (Vinayachandran and Curian, 2008). The local surface water $\delta^{18}O$ is sensitive to change SSS, and can be extracted from the isotopic signal of planktonic foraminifera when its SST component is estimated from Mg/Ca ratios. In modern conditions, the SST cooling associated with increased (decreased) SSS reflects relatively stronger winter (summer) monsoon.

A low salinity plume originating in the eastern coastal region of India (western BoB) during the post summer monsoons (i.e., Winter-Fall) travels around Sri-Lanka, enters into southern-EAS and penetrates northward up to 15^{o}N latitude (off Goa) as a low-salinity tongue (Figure 1). This tongue is quite wide (~400 km) at the entry point (southern-EAS) and narrows as it travels northward. The cause of this low-salinity plume is attributed to the higher sea level in BoB than in the Arabian Sea and the prevailing wind system in the region (Shankar and Shetye, 2001). The BoB receives 50 times more freshwater (~100,000 m^3/s) than the EAS (~200 m^3/s) during the summer monsoon (University of Wisconsin-Madison, 2010). This in turn establishes alongshore density gradient and differing sea levels between the east (high) and west coast (low) of India resulting in intense poleward flowing plume of low salinity water into the EAS following the summer monsoons. As a consequence, ~6 Sv of low- salinity BoB water is advected into the EAS (Shankar 2000), which is already preconditioned with lowered salinity due to summer monsoon overhead precipitation and seasonal outflow of medium to small rivers draining the Deccan Mountains. Hence, the EAS is distinctly marked with low-salinity water bounded to the north and west by high-salinity waters characteristic of the Arabian Sea (HSW). The SSS in this low-

salinity tongue gradually increases from southern-EAS as it moves poleward and becomes indistinguishable at central-EAS (off Goa) due to overwhelming influence of HSW. Thus, the dynamics of this low-salinity plume in the EAS is dictated by the Indian monsoon system. Therefore, the temporal variation in the north-south SSS gradient in this low salinity tongue may be useful to understand the past changes in relative intensities of summer and winter monsoons. Keeping the river discharge and overhead precipitation driven freshening of the Arabian Sea and BoB as a basis, the relative increase in summer monsoons would strengthen the low-salinity tongue in the EAS; While, the relative weakening of summer monsoons would tend to reduce the SSS contrast between the two basins or weaken this tongue. This forms the preamble for the present study.

Here, we report the past changes in North-South SSS-gradient within the low-salinity tongue to understand variability of summer and winter monsoons since the Last Glacial Maximum (LGM). For this, two sediment cores collected at two ends of the low-salinity tongue are used. The northern core is located presently at the termination of low-salinity tongue where influence of HSW is distinctly evident by SSS of >36 psu and narrow low SSS band (<100 km wide). The southern core, on the other hand, is located at the entry of low-salinity tongue, which is evident by distinctly low-SSS water (<35 psu) and broad low-SSS band (>400 km wide) (Figure 1). Paired measurements of $\delta^{18}O$ and Mg/Ca in *G. Sacculifer* (without terminal sac) were utilized to estimate SST and $\delta^{18}O_{seawater}$ to reconstruct past changes in the SSS.

Materials and Methods

The upper 150 cm section of two ~5 m long sediment cores from EAS (SK117/GC08 and SK129/CR04: Figure 1) were used for the present study. The former core was collected at 15°29.67'N & 71°00.98'E (henceforth 'northern location') and the latter at 06°29.65'N & 75°58.68'E (henceforth 'southern location' for convenience). The water depths at these two locations are 2500 and 2000 m respectively. The sediment cores were sub-sampled at 2 cm intervals. The depth in sediment cores was translated into calendar ages based on eight (per sediment core) reservoir corrected (600 y for the study region: http://calib.qub.ac.uk/marine/) AMS ^{14}C dates calibrated using on-line HULU calibration program (Danzeglocke et al., 2007) (Table 1), and estimated linear sedimentation rates between two dated sections (Figure 2). The core-top age for northern location core is 2259 ± 64 y BP and for southern

core is 3048 ± 67 y BP. The last dated sections correspond to 34124 ± 402 and 32564 ± 386 y BP respectively. Thus complete LGM and most part of the Holocene period is retrieved.

The *G. sacculifer* is a spinose mixed-layer dwelling planktic foraminifer (Hembleben et al., 1989) calcifying in a narrow depth range of 25-40 m (Farmer et al., 2007), which is relatively more resistant to dissolution compared to other planktic foraminifera (Dekens et al., 2002; Delaney et al., 1985), having nearly uniform inter-chamber distribution of Mg and Ca (Eggins et al., 2003). Previously published $\delta^{18}O$ data for both the sediment cores (Banakar et al., 2005; Chodankar et al., 2005) and paired Mg/Ca SST for the northern location core (Banakar et al., 2010) were available for the present study. To obtain paired data, for southern location core, the depth sections and size of the tests for Mg/Ca measurement were maintained the same as those previously used for generating $\delta^{18}O$ time-series.

Around sixty visibly clean and intact tests of *G. sacculifer* from a size range of 255 to 350 μm were picked from the southern location core under binocular microscope for cleaning following the procedure outlined by Barker et al. (2003). The measurements were performed using intensity-ratio calibration techniques (De Villiers et al., 2002) with five multi-element calibration standards. The Mg/Ca was measured on a Perkin Elmer 2000 DV sequential ICP-OES facility at the National Institute of Oceanography. A quality control (QC) solution with 5.144 mmol/mol of Mg/Ca was run after every six samples to check the instrumental consistency. Forty measurements of the QC spread over the analytical period yielded a mean of 5.126 ± 0.097 mmol/mol respectively, suggesting that the Mg/Ca data presented here is of high precision. The Fe, Mn and Al were also measured in order to monitor contamination by clays and oxides. The Fe/Ca, Al/Ca and Mn/Ca were mostly <0.3 mmol/mol and their scatter plots versus Mg/Ca yielded insignificant correlations ($R^2 < 0.3$), together indicating contamination free Mg/Ca data. The analytical protocol for previously published Mg/Ca-$\delta^{18}O$ is available in Banakar et al. (2010).

The Mg/Ca ratios (mmol/mol) were converted into calcification temperatures using Dekens et al., (2002) tropical pacific calibration equation (Mg/Ca = 0.37 exp 0.09[T – 0.36(core depth in km) - 2 °C]) for *G. sacculifer*. Since there is no calibration equation available for the Indian Ocean, this calibration was preferred as, a) it was species specific, b) the ocean-atmosphere coupled phenomenon over the northern Indian Ocean and western Pacific are similar (Webster and Fasullo, 2002), and c) the western Pacific and the tropical Indian Ocean are well connected. The latter two reasons, at the outset,

appear to be the hydrographic factors that have caused simultaneous termination of *G. ruber (pink)* only from tropical Indo-Pacific ~125 kyr ago (Thompson et al., 1979). The sea level corrected $\delta^{18}O_{G.sacculifer}$ (Shackleton, 2000) was translated into $\delta^{18}O_{SEAWATER}$ using Epstein et al. (1953) paleotemperature equation [$T(°C) = 16.9 - 4.4\ (\delta^{18}O_{G.sacculifer} - \delta^{18}O_{SEAWATER}) + 0.1\ (\delta^{18}O_{G.sacculifer} - \delta^{18}O_{SEAWATER})^2$]. Although, the time-series of global ice volume of Shackleton (2000) is not based on the radiocarbon age control, it is one of the robust ice-volume datasets available for the ice-volume (sea-level) correction. The $\delta^{18}O_{SEAWATER}$ was further converted into local-SSS using Dahl and Oppo, (2002) empirical equation ($y = 0.57x - 20$; where y = Salinity and x = Residual $\delta^{18}O_{SEAWATER}$). The complete dataset is presented in Appendix. Although, the estimated salinity from $\delta^{18}O_{SEAWATER}$ has uncertainties (Rohling et al., 2007; estimated error on the present data is ~1 psu), it is more convenient to appreciate changes in salinity than changes in corresponding $\delta^{18}O_{SEAWATER}$.

Results and Discussions

The studied sections of the sediment cores cover a period between Marine Isotope Stage (MIS)-3 and the Holocene. The LGM, as indicated by the heaviest $\delta^{18}O_{G.\ sacculifer}$ (± measurement precision of 0.08‰), spans 26 to 18 ka BP. The MIS 1/2 and MIS 2/3 boundaries are evident at 13 and 29 ka BP, which is consistent with LR04 benthic stack (Lisiecki and Raymo, 2005), and the timing of the LGM's ice-dynamics (Clarke et al., 2009). The $\delta^{18}O_{G.sacculifer}$ ranges between 0.4 ‰ (LGM) and -1.6 ‰ (Holocene) in northern location and between 0 ‰ to -2‰ in southern location (see Appendix). In the former location, the $\delta^{18}O_{G.sacculifer}$ remained heavier than in the latter location throughout the dated interval (see Figure 3), indicating the existence of north-south SSS gradient in the past also, considering nearly similar changes in SSTs at both core-locations. The LGM-Holocene $\delta^{18}O_{G.sacculifer}$ contrast in both sediment cores is ~2 ‰, of which, 1.2 ‰ could be accounted for global ice volume change (Shackleton, 2000). The reminder of ~0.8 ‰ would therefore was caused by changes in ambient local-SST and -SSS). The $\delta^{18}O_{G.sacculifer}$ in both the records exhibit monotonous decrease from ~18 ka BP to attain Holocene optimum at ~8 ka BP. This 10 kyr period is the well known transition of global climate from cold-to-warm surrounding the Termination-1.

The Mg/Ca ratios vary between 3 and 4 mmol/mol (see Appendix), which is within the expected range for tropical oceans (Lea et al., 2000; Barker et al., 2005; Saraswat et al., 2005; Dahl and Oppo, 2006). This Mg/Ca range yields a SST range of 27^{o} to 29°C in the EAS (see Appendix). The core-top

SSTs are 29°C and 28.6°C for northern- and southern- location respectively and are closely comparable to the modern SSTs in those locations (see www.noaa.nodc.gov/woa2009) (Figure 1). The LGM-Holocene maximum SST gradient is ~2°C, while the average LGM-Holocene gradient is only 1°C. This smaller average gradient is the result of intermittent warming events during the cold-LGM and cooling events during the warm-Holocene. However, the maximum 2°C shift in the LGM-to-Holocene SSTs is comparable to various published stacked SST records for tropical oceans (CLIMAP 1981; MARGO 2009; PMIP2 - Bette et al., 2009).

The SST time-series of both sediment cores exhibit step increase from the LGM-low (27°C) to Holocene-high (29°C) (see Appendix). Within the Holocene, the SST indicates a decrease of ~1°C at ~ 8 ka BP. The increase was rapid until reaching the Holocene optimum (~15-14 ka BP), after a stable condition between 17 and 15 ka BP (Figure 4). Step-increases have also been observed in other Arabian Sea SST time-series at around 15-12 ka BP (Saher et al., 2007; Anand et al., 2008), making this feature typical of deglacial Arabian Sea SST evolution. We speculate that, the step-increases in SSTs through the deglacial warming may be a necessity for sea surface-preconditioning before another warming event in partially land-locked seas, where two bodies (land and ocean) with large difference in heat capacity need to respond simultaneously to similar climate-change forcing. The lowest SSTs are observed between 27 and 22 ka BP in both the locations compared to pre-LGM (32-29 ka BP) moderately warmer SSTs. The lowest - SST time slice is in agreement with the ice growth dynamics during the LGM, where rapid expansion in global ice began ~33 ka BP to reach peak growth at ~26.5 ka BP, establishing LGM conditions that lasted until ~20 ka BP (Clark et al., 2009). In light of this global ice evolution, a 2°C SST cooling in EAS was the result of global climate forcing.

The variations in EAS-SST time-series do not exhibit smooth structure, but show fluctuations as much as 1˚C within the LGM period itself and are more distinct than the marginal variations exhibited by $\delta^{18}O_{G.sacculifer}$ (± 0.2 ‰), $\delta^{18}O_{SEAWATER}$ (± 0.2 ‰) or SSS (± 0.2 psu) (Figure 5). Similar warming events within the LGM were also observed in other Mg/Ca SST records of the Arabian Sea (Table 2 and Figure 6: Saher et al., 2007; Anand et al., 2008; Banakar et al., 2010; Govil and Naidu, 2010; Mahesh et al., 2011), indicating that the tropical ocean SSTs were not continuously colder throughout the LGM, but were punctuated by short-term warmer events. The resultant of few consecutive interstadials of D-O oscillations with comparable time-slices causing the observed warm events within the LGM is unlikely, because, similar responses are not seen in $\delta^{18}O_{G.sacculifer}$ time-series. Therefore, the most likely cause of

SST warming events in the LGM-EAS appears to be intermittent weakening of glacial winters. As the winters during glacial periods are more intense and prolonged than during the interglacials (Prell and Van Campo, 1986), and also have profound influence on SSTs of the Arabian Sea (Fontugne and Duplessy, 1986), even a short-term weakening of winter monsoons would induce distinct warming of the SST in the northern Indian Ocean as a whole. Further, Figure 6 shows comparable events of ~8 ka cooling, beginning of deglaciation, and glacial cooling in the entire EAS, but there are other warming events with timing offsets at different locations within the EAS. Such behavior of SST time series from the EAS probably suggests geographically variable local climatology. The ecosystem modeling for the Arabian Sea (Murtugudde et al., 2007) clearly brings out the effect of wind stress and wind speed in driving the surface climatology that changes from coast to open ocean under similar monsoon forcing. The locally variable wind stress curls during the strong monsoons could result in downwelling in some parts leading to deepening of the mixed layer resulting in entrainment cooling. Hence, ocean dynamics might be driving the surface temperatures rather than evaporative cooling forced by strong monsoon winds alone (Murtugudde et al., 2007).

The SSS estimates from core-top sections of the northern- and southern- locations are 36.2 and 35.6 psu respectively, which are nearly similar to the modern SSS at those locations (see Figure 1b) with a modern north-south gradient of ~0.6 psu. The SSS reduction from LGM to Holocene at northern location is 1.5 psu and at southern location is 1 psu, i.e., the SSS shift from LGM to Holocene in northern-EAS was 0.5 psu more than that at the southern-EAS. Further, the north-south SSS gradient during LGM was 1.2 psu and that decreases to 0.7 psu during the Holocene. These distinct location specific and spatial changes in SSS at the outset could be attributed to significantly different SSS structure during the LGM as compared to the Present (Holocene). Presently, the northern location is influenced partially and the southern location totally by the low-salinity tongue. The 0.5 psu higher change from LGM to Holocene in the northern location and 0.5 psu larger north-south gradient during the LGM together suggest a probable withdrawal of the low salinity tongue from the northern location. This scenario requires considerable reduction of sea level difference between East Coast (BoB) and West Coast (EAS) of India, which is feasible only if the E-P of the BoB is significantly increased. Such drastically different surface climatology of the LGM-BoB indicates considerably weakened summer monsoons and strengthened winter monsoons. The reduced north-south SSS gradient during the Holocene (Figure 5), on the other hand, suggests strengthened low-salinity tongue due to reduced-salinity-water inflow from BoB, i.e., intensification of summer monsoons. This observation based on the

dynamics of the low-salinity tongue is consistent with monsoon proxy stack of Clemens and Prell (2003). The strengthening of low-salinity tongue would push back the northern Arabian Sea HSW-front resulting in reduced influence of high salinity water on the northern location. This is possible when the sea level in BoB is significantly higher than in the EAS and Western Ghats (Deccan Mountains) river discharge to the EAS is increased. In light of modern observations such hydrological conditions are typical of intensified summer monsoons.

The deglaciation in EAS is marked by rapid reduction in SSS at both locations between ~18 and 10 kyr BP to reach their respective Holocene average values (Figure 5). Significant reduction in SSS (>1 psu) of the EAS within 8 kyr of this transition is a clear indication of rapid intensification of summer monsoons along with weakening of winter monsoons. That is, the deglacial transition has brought-in significant reorganization in the Indian monsoon system. The optimum SSTs in the EAS were attained between 13 and 14 ka BP (Figure 4), while SSS minima attained at ~8 ka BP (Figure 5), producing an offset in timings of two important climatological parameters. The SST warming initiating strengthening of summer monsoon convections over the Arabian Sea appear to have established few thousand of years before the actual intensification of the summer monsoons. Such SST pre-conditioning may be a requirement of the Indian monsoon system during major shift in climate from glacial to interglacial conditions.

Summary

The last ~32 ky records of surface climatology in the low salinity tongue of Eastern Arabian Sea contain important clues for past variability in the Indian monsoon system. While the SST changes from the Last Glacial Maximum to Holocene were nearly uniform at the northern and southern ends of that tongue, the surface salinity shift was higher at the northern end suggesting altogether different surface salinity structure in the EAS during the glacial maximum. The north-south surface salinity gradient was also different during the LGM as compared to the Holocene. The increased N-S salinity gradient during the LGM indicates diminished low-salinity tongue, probably caused by significantly weakened summer monsoon freshwater flux to the Bay of Bengal and increased winter evaporation in the Arabian Sea. Therefore, high-resolution reconstruction of variation in the salinity structure of the coastal Eastern Arabian Sea could be a powerful tool to understand the precise variation in the relative intensities of summer and winter monsoons.

Acknowledgements

We thank Mitzi De'Martino of Arizona University for measuring radiocarbon. Anjali Chodankar is thanked for permitting us to use published oxygen-isotope data. The samples for the present study were collected with the support of Ministry of Earth Sciences on board their research vessel ORV. Sagar Kanya. BSM thanks CSIR-HRDG for providing him junior and senior research fellowships.

References

Anand, P., Kroon, D., Singh, A.D., Ganeshram, R.S., Ganssen, G., and Elderfield, H., 2008. Coupled sea surface temperature–seawater $\delta^{18}O$ reconstructions in the Arabian Sea at the millennial scale for the last 35 ka. *Paleoceanography,* 23: PA4207.

Banakar, V. K., Mahesh, B. S., and Burr, G., 2010. Climatology of the Eastern Arabian Sea during the last glacial cycle reconstructed from paired measurement of foraminiferal $\delta^{18}O$ and Mg/Ca. *Quaternary Research*, **73**: 535-540.

Barker, S., Cacho, I., Benway, H., and Tachikawa, K., 2005. Planktonic foraminiferal Mg/Ca as a proxy for past oceanic temperatures: a methodological overview and data compilation for the last glacial maximum. *Quaternary Science Reviews*, **24**: 821-834.

Barker, S., Greaves, M., and Elderfield, H., 2003. A study of cleaning procedure used for foraminiferal Mg/Ca paleothermometry. *Geochemistry Geophysics Geosystems*, **4**: 8407.

Clark, P.U., Dyke, A.S., Shakun, J.D., Carlson, A.E., Clark, J., Wohlfarth, B., Mitrovica, J., Hostetler, S.W., and McCabe, A.M., 2009. The Last Glacial Maximum. *Science,* **325**: 710-714.

CLIMAP Project Members, 1981. Seasonal reconstruction of the Earth's surface at the last glacial maximum Map Chart Ser. MC-36, *Geological Society of America.*

Chodankar, A.R., Banakar, V.K., and Oba, T., 2005. Past 100 ky surface salinity gradient response in the Eastern Arabian Sea to the summer monsoon variation recorded by $\delta^{18}O$ of *G. sacculifer*. *Global Planetary Change*, **47**: 135-142.

Dahl, K.A., and Oppo, D.W., 2006. Sea surface pattern reconstructions in the Arabian Sea. *Paleoceanography*, **21**: PA1014.

Danzeglocke, U., Jöris, O., and Weninger, B., 2009. CalPal-2007^{online}. http://www.calpal-online.de/, 2008-10-05.

Dekens, P.S., Lea, D.W., Pak, D.K., and Spero, H.J., 2002. Core-top calibration of Mg/Ca in tropical foraminifera: refining paleo-temperature estimation. *Geochemistry Geophysics Geosystems*, **3**: 1022.

Delaney, M.S., Be, A.W., and Boyle, E.A., 1985. Li, Sr, Mg and Na in foraminiferal calcite shells from laboratory culture, sediment traps

De Villiers, S., Greaves, M., and Elderfield, H., 2002. An intensity ration calibration method for the accurate determination of Mg/Ca and Sr/Ca of marine carbonates by ICP-AES. *Geochemistry, Geophysics, Geosystems*, **3**: 2001GC000169.

Eggins, S., De Deckker, P., and Marshall, J., 2003. Mg/Ca variation in planktonic foraminifera tests: implications for reconstructing palaeo-seawater temperature and habitat migration. Earth and Planetary Science Letters, **212**: 291-306.

Epstein, S., Buchsbaum, R., Lowenstam, H. A., Urey, H. C., 1953. Revised carbonate-water isotopic temperature scale. *Bulletin of Geological Society of America*, **64**: 1315-1325.

Farmer, E. C., Kaplan, A., de Menocal, P. B. and Lynch-Stieglitz, J., 2007. Corroborating ecological depth preferences of planktonic foraminifera in the tropical Atlantic with the stable oxygen isotope ratios of core-top specimen. *Paleoceanography,* 22: PA3205.

Fontugne, M.R., and Duplessy, J.C., 1986. Variations of the monsoon regime during the upper Quaternary: Evidence from carbon isotopic record of organic matter in north Indian Ocean sediment cores. *Palaeogeography Palaeoclimatology Palaeoecology,* **56**: 69-88.

Govil, P., and Naidu, P.D., 2010. Evaporation-precipitation changes in the eastern Arabian Sea for the last 68 ka: Implications on monsoon variability. *Paleoceanography,* **25**: PA1210.

Hemleben, C., Spindler, M. and Anderson, O.R. 1989. *Modern planktonic foraminifera*. Springer-Verlag, New York, N.Y.

Lisiecki, L.E., and Raymo, M.E., 2005. A Pliocene-Pliestocene stack of 57 globally distributed benthic $\delta^{18}O$ records. *Paleoceanography*, **20**: PA1003.

Lea, D.W., Mashiotta, T.A., Spero, H.A., 1999. Controls on magnesium and strontium up-take in planktonic foraminifera determined by living culturing, *Geochimica et Cosmochimica Acta*, **63**: 2369-2379.

Mahesh, B., Banakar, V.K., and Burr, G., 2011. Paired Measurements of Foraminiferal δ18O and Mg/Ca Ratios of Indian Monsoons Reconstructed from Holocene to Last Glacial Record. *Acta Geologica Sinica*, **85**: 950–956.

MARGO Project Members, 2009. Constraints on the magnitude and patterns of ocean cooling at the Last Glacial Maximum. *Nature Geoscience*, **2**:127-132.

Murtugudde, R., Seager, R., and Thoppil, P., 2007. Arabian Sea response to monsoon variations. *Paleoceanography,* **22**: PA4217.

Otto-Bliesner, B.L., Schneider, R., Brady, E.C., Kucera, M., Abe-Ouchi, A., Braconnot, P., Crucifix, M., Hewitt, C., Kageyama, M., Marti, O., Paul, A., Rosell-Melé, A., Weber, S.L., Weinelt, M., and Yu, Y., 2009. A comparison of PMIP2 model simulations and the MARGO proxy reconstruction for tropical sea surface temperatures at last glacial maximum. *Climate Dynamics*, **32**: 799-815.

Prasanna Kumar, S., and Prasad, T.G., 1999. Formation and spreading of Arabian Sea high salinity water mass. *Journal of Geophysical Research*, **104**: 1455-1461.Prell, W.L., and Van Camp, E., 1986. Coherent response of Arabian Sea upwelling and pollen transport to late Quaternary monsoonal winds. ***Nature,* 323:** 526 - 528.

Prell, W.L., and Van Camp, E., 1986. Coherent response of Arabian Sea upwelling and pollen transport to late Quaternary monsoonal winds. ***Nature,* 323:** 526 - 528.

Rohling, E.J., 2007. Progress in paleosalinity: Overview and presentation of a new approach. *Paleoceanography*, **22**: PA3215.

Saher, M.H., Jung, S.J.A., Elderfield, H., Greaves, M., and Kroon, D., 2007. Sea surface temperatures of the western Arabian Sea during the last deglaciation. *Paleoceanography,* **22**: PA2208.

Saraswat, R., Nigam, R., Weldeab, S., Mackensen, A., and Naidu, P.D., 2005. A first look at past sea surface temperatures in the equatorial Indian Ocean from Mg/Ca in foraminifera. *Geophysical Research Letters*, **32**: L24605.

Shackleton, N.J., 2000. The 100,000 year ice-age cycle identified and found to lag temperature, carbon dioxide and orbital eccentricity. *Science,* **289**: 1897-1902.

Shankar, D., 2000. Seasonal cycle of sea level and currents along the coast of India. *Current Science*, **78**:279-288.

Shankar, D., and Shetye, S.R., 2001. Why is mean sea level along the Indian coast higher in the Bay of Bengal than in the Arabian Sea? *Geophysical Research Letters*, **28**: 563-565.

Shetye, S.R., Gouveia, A.D., Shenoi, S.S.C., Michael, G.S., Sundar, D., Almeida, A.M.,and Santanam, K., 1991. The coastal current off western India during thenortheast monsoon. *Deep Sea Research Part A. Oceanographic Research Papers*, **38**: 1517-1529.

Thompson, P.R., Be`, A.W.H., Duplessy, J., and Shackleton, N.J., 1979. Disappearance of pink-pegmented *Globigerinoides ruber* at 120,000 yr BP in the Indian and Pacific Oceans. *Nature*, **280**: 354-358.

Wilson-Diaz, D., Mariano, A.J., and Evans, R.H., 2009. On the heat budget of the Arabian Sea. *Deep Sea Research Part I: Oceanographic Research Papers*, **56**: 141-165.

Webster, P.J., and Fasullo, J., 2002. Monsoons-Dynamic theory, in: Encyclopedia of atmospheric Sciences. *Academic Press*, **3**: 1370-1385.

Figure captions

Figure 1. Location of the studied sediment cores (filled circles) are shown on both annual surface temperature (a) and surface salinity (b) distribution maps (www.noaa.nodc.gov). The locations of the other published Mg/Ca-SST records are shown with open circles on SST map (a). Highly simplified trajectories of seasonally reversing monsoon winds are shown with shaded gray arrows on annual salinity map (b). The thickness of arrow indicates relative strength of modern summer (thick = strong) and winter (thin = weak) monsoons. Climate stage averaged surface salinity values at the studied core locations are shown with white fonts (Last Glacial Maximum) and black font (Holocene). The low-salinity water advection into the EAS from BoB is shown with a broken arrow.

Figure 2. Depth versus age in the studied sediment cores. The radiocarbon dated sections are shown with red arrows along with corresponding age on X-axis. T1 = Termination 1 or MIS1/MIS2. 2/3 = MIS2/MIS3 climate boundaries.

Figure 3. Time-series of $\delta^{18}O_{G.sacculifer}$ and ice-volume corrected $\delta^{18}O_{G.sacculifer}$ in northern (GC08) and southern (CR04) sediment cores compared with LR04 Benthic Stack (Lisiecki and Raymo, 2005) and SPECMAP (Imbrie et al., 1984). The curve used for ice-volume correction (Shackleton, 2000) is also shown in panel 3 from top. Broken vertical lines indicate marine isotope stage boundaries and beginning of deglaciation identified in the studied sediment cores. The black and red color filled squares on LR04 and SPECMAP respectively indicate MIS1/2 and 2/3 in those reference records.

Figure 4. The time-series of measured Mg/Ca in *G. sacculifer* along with 1σ standard error bars and estimated Mg/Ca-SST for northern (GC08)- and southern (CR04) locations of the low-salinity tongue.

Figure 5. The time-series of $\delta^{18}O_{SEAWATER}$ (estimated from residual $\delta^{18}O_{G.sacculifer}$ and SST) and sea surface salinity (estimated from $\delta^{18}O_{SEAWATER}$) in the northern [high-salinity end (GC08: red curve)] and southern [low-salinity end (CR04: blue curve)] locations of the low-salinity tongue.

Figure 6. Comparison of present Mg-SST time-series with previously published reconstructions. SK129/CR-04 is the new core utilized for the present study (Core Number enclosed within box). Other SST time-series are published records (see Table 2). Although general structures of variation in the above time-series are comparable, there are minor events showing timing and amplitude (see discussion).

CAPTIONS TO TABLES

Table 1. Details of the sections dated by AMS-radiocarbon along with the laboratory references.

Table 2. Comparison of available SST gradients estimated from Mg/Ca Palaeothermometry for the Eastern Arabian Sea locations.

Appendix: $\delta^{18}O$, Mg/Ca, SST and SSS data for the two sediment cores utilized in the present study.

Figure 1 (BSM-VKB)

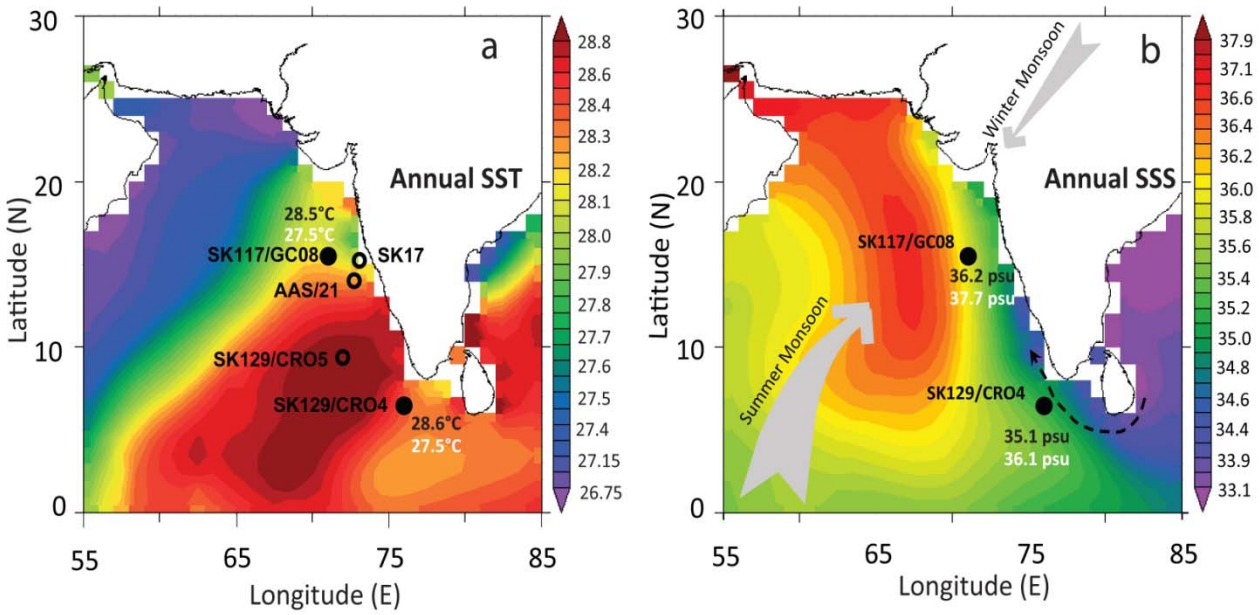

Figure 2 (BSM-VKB)

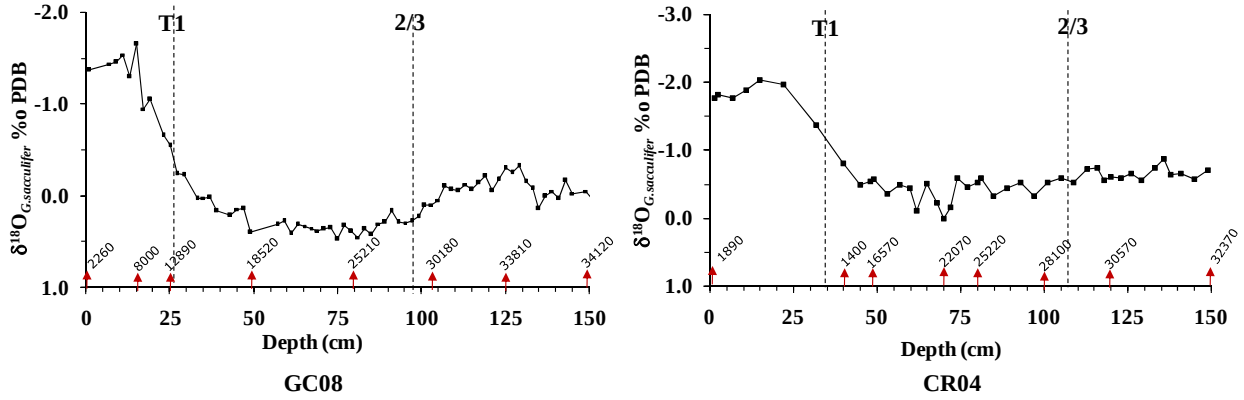

Figure 3 (BSM-VKB)

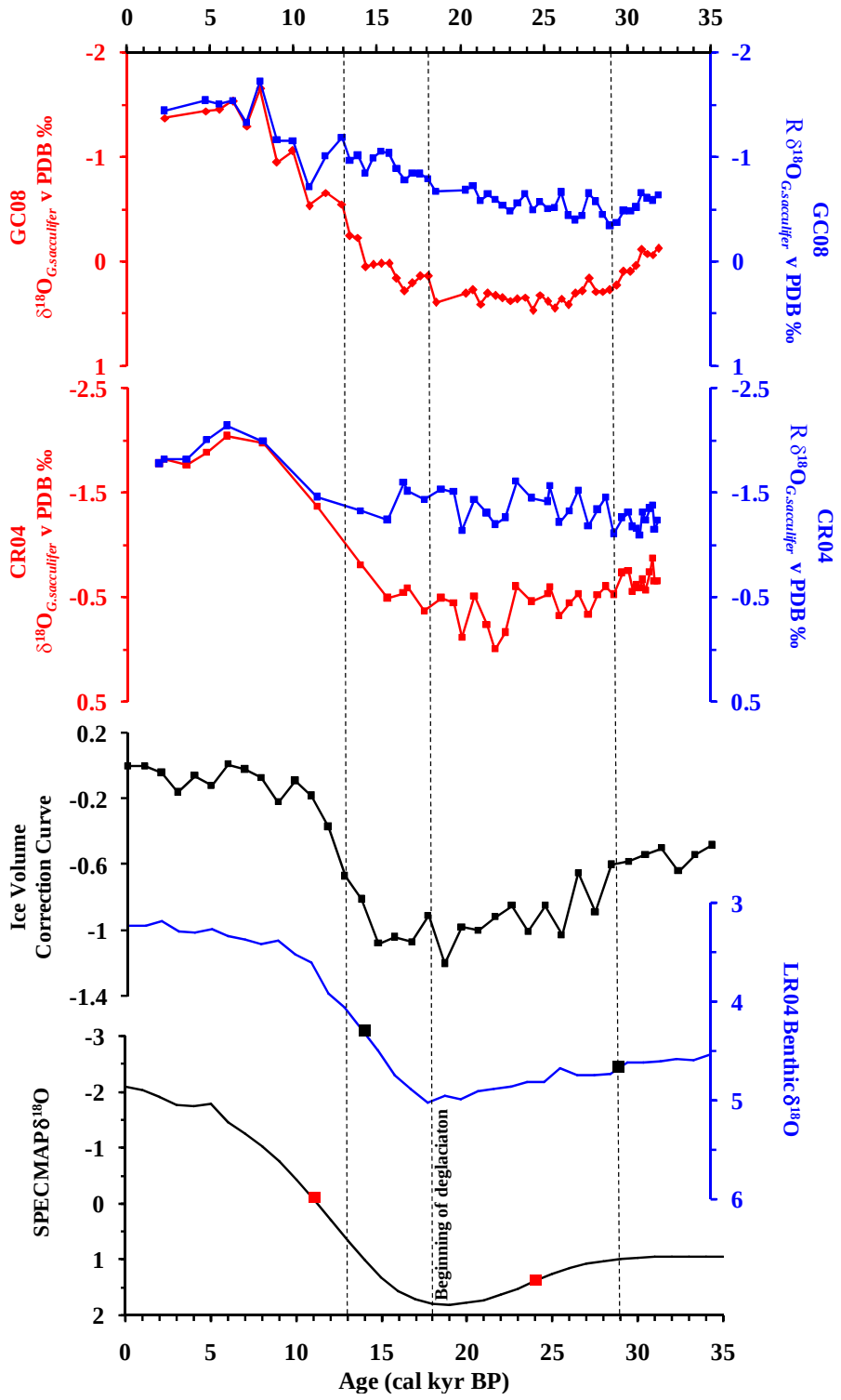

Figure 4 (BSM-VKB)

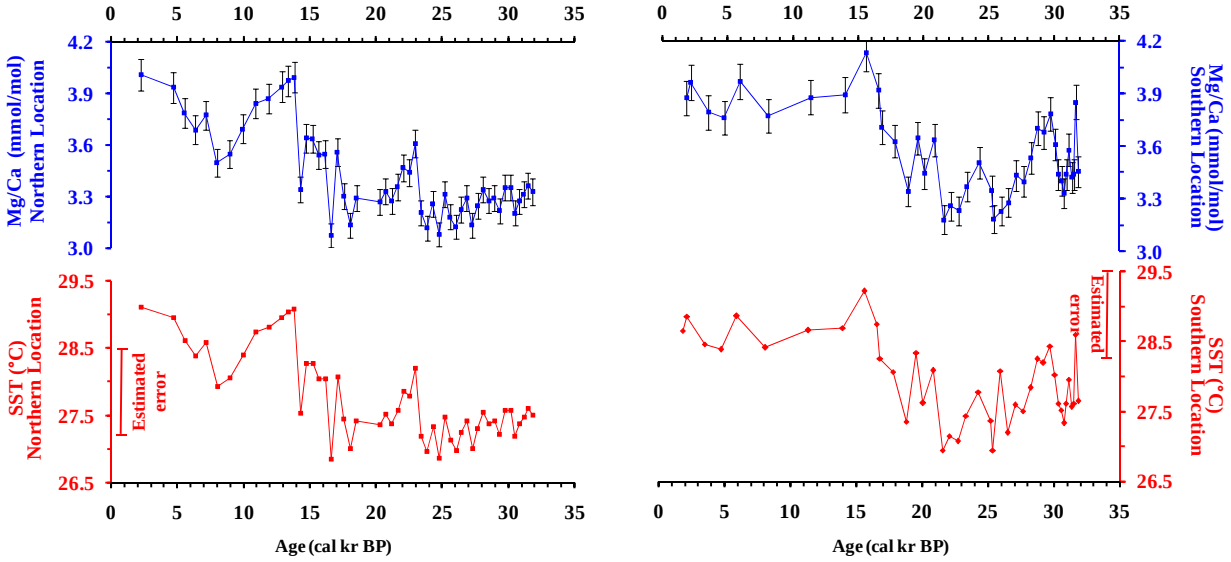

Figure 5 (BSM-VKB)

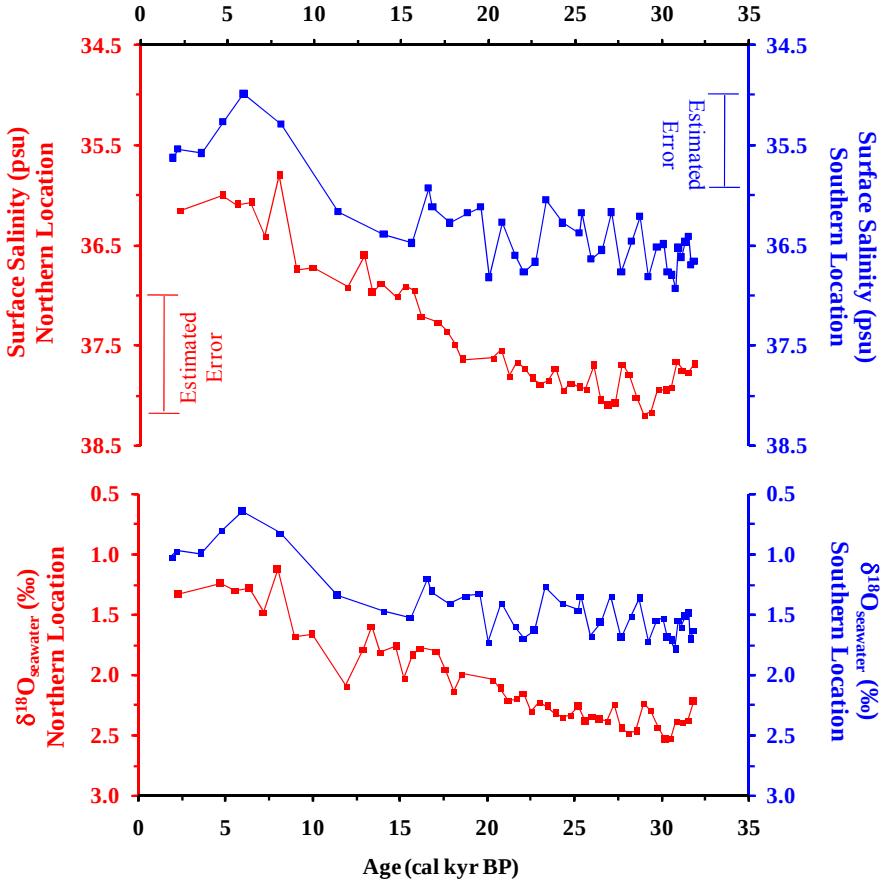

BSMVKB: FIGURE 6

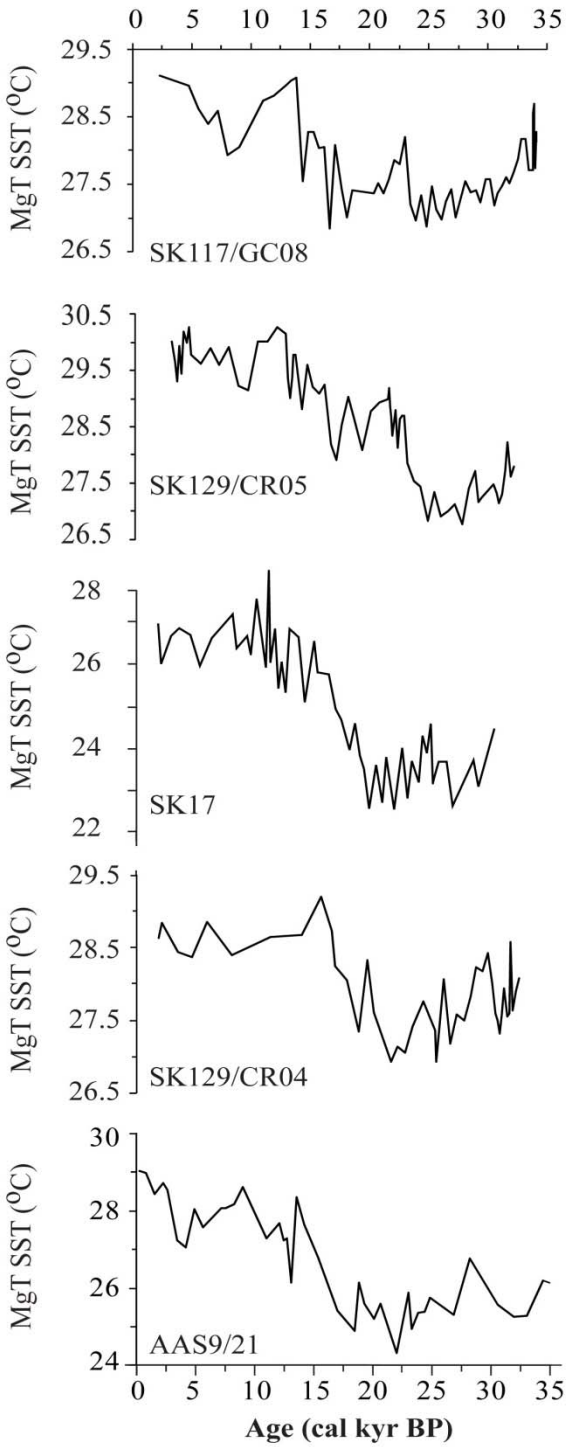

Table 1 (BSM-VKB)

Sample Code	Depth in Core (cm)	Lab code		^{14}C Measured Age		* Calendar Age	
		AA	LAB #	yr BP	± yr	Cal yr BP	± yr
SK117/GC08	1	1566	Utrecht	2847	26	2259	64
	15	AA79596	X10218A	7775	52	8000	37
	25	AA79597	X10219A	11546	74	12887	100
	49	AA79598	X10220	16031	91	18519	298
	79	AA79599	X10221	21660	150	25214	393
	103	AA79600	X10222A	25910	230	30180	230
	125	AA79601	X10223	30140	450	33805	433
	149	AA79602	X10224	30550	460	34124	402
SK129/CR04	1.5	AA79603	X10225	2533	38	1885	42
	20	AA79604	X10226	7144	53	7466	38
	40	AA79605	X10227	12616	85	14005	224
	48	AA79606	X10228	14190	110	16563	383
	70	AA79607	X10229	19060	120	22073	327
	80	AA79608	X10230	21660	360	25216	535
	100	AA79609	X10231	23940	190	28100	243
	120	AA79611	X10233	26160	260	30556	481
	150	AA79610	X10232	28370	340	32369	364

Table 2. (BSM-VKB)

Core ID	Sediment core details			SST		Δ°C	Reference
	Lat.	Long.	Water Depth (m)	LGM Avg.	Holocene Avg.		
SK17	15° 15`	72° 58`	840	23°C	27°C	4°C	Anand et al., 2008
SK117/GC08	15° 29`	71° 00`	2500	27°C	29°C	2°C	Banakar et al., 2010
AAS9/21	14° 30`	72° 39`	1807	25°C	28°C	3°C	Govil and Naidu, 2010
SK129/CR05	9° 21`	71° 59`	2300	27°C	29.5°C	2.5°C	Mahesh et al., 2011
SK129/CR04	6° 29`	75° 58`	2000	27°C	29°C	2°C	Present Study

Appendix

SK117/GC08

Calendar Age ky cal BP	**Mg/Ca mmol/mol**	**SST (°C)**	**$\delta^{18}O_{G.sacculifer}$ v PDB ‰**	**Salinity (psu)**
2.26	4.009±0.09	29.1±0.7	-1.369	36.2
4.72	3.937±0.09	29.0±0.7	-1.436	36.0
5.54	3.789±0.09	28.6±0.7	-1.453	36.1
6.36	3.688±0.08	28.4±0.6	-1.532	36.1
7.18	3.774±0.09	28.6±0.6	-1.294	36.4
8.00	3.496±0.08	27.9±0.6	-1.650	35.8
8.98	3.547±0.08	28.1±0.6	-0.946	36.7
9.95	3.693±0.08	28.4±0.6	-1.053	36.7
10.93	3.843±0.09	28.7±0.7	-0.530	37.4
11.91	3.871±0.09	28.8±0.7	-0.654	36.9
12.89	3.940±0.09	29.0±0.7	-0.545	36.6
13.36	3.975±0.09	29.0±0.7	-0.241	37.0
13.83	3.995±0.09	29.1±0.7	-0.225	36.9
14.30	3.338±0.08	27.5±0.6	0.052	37.3
14.76	3.640±0.08	28.3±0.6	0.032	37.0
15.23	3.637±0.08	28.3±0.6	0.022	36.9
15.70	3.542±0.08	28.0±0.6	0.019	37.0
16.17	3.545±0.08	28.0±0.6	0.165	37.2
16.64	3.073±0.07	26.8±0.6	0.286	37.5
17.11	3.556±0.08	28.1±0.6	0.210	37.3
17.58	3.301±0.08	27.4±0.6	0.144	37.4
18.05	3.132±0.07	27.0±0.6	0.140	37.5
18.52	3.290±0.07	27.4±0.6	0.396	37.6
20.30	3.268±0.07	27.4±0.6	0.308	37.6
20.75	3.330±0.08	27.5±0.6	0.278	37.5
21.19	3.273±0.07	27.4±0.6	0.411	37.8
21.64	3.355±0.08	27.6±0.6	0.311	37.7
22.08	3.467±0.08	27.9±0.6	0.328	37.7
22.53	3.440±0.08	27.8±0.6	0.352	37.8
22.98	3.609±0.08	28.2±0.6	0.378	37.9
23.42	3.204±0.07	27.2±0.6	0.363	37.9
23.87	3.115±0.07	27.0±0.6	0.347	37.7
24.31	3.257±0.07	27.3±0.6	0.470	37.9
24.76	3.080±0.07	26.9±0.6	0.326	37.9
25.21	3.312±0.08	27.5±0.6	0.386	37.9

25.62	3.180±0.07	27.1±0.6	0.450	37.9
26.04	3.122±0.07	27.0±0.6	0.358	37.7
26.45	3.224±0.07	27.2±0.6	0.421	38.0
26.87	3.291±0.07	27.4±0.6	0.307	38.1
27.28	3.132±0.07	27.0±0.6	0.285	38.1
27.69	3.245±0.07	27.3±0.6	0.168	37.7
28.11	3.341±0.08	27.5±0.6	0.290	37.8
28.52	3.276±0.07	27.4±0.6	0.293	38.0
28.94	3.289±0.07	27.4±0.6	0.277	38.2
29.35	3.216±0.07	27.2±0.6	0.228	38.2
29.76	3.353±0.07	27.6±0.6	0.102	37.9
30.18	3.351±0.07	27.6±0.6	0.098	37.9
30.51	3.202±0.07	27.2±0.6	0.046	37.9
30.84	3.271±0.07	27.4±0.6	-0.109	37.7
31.17	3.313±0.07	27.5±0.6	-0.070	37.7
31.5	3.363±0.07	27.6±0.6	-0.060	37.8
31.83	3.327±0.07	27.5±0.6	-0.124	37.7

SK129/CR04

Calendar Age ky cal BP	**Mg/Ca mmol/mol**	**SST (°C)**	**$\delta^{18}O_{G.Sacculifer}$ v PDB ‰**	**Salinity (psu)**
1.89	3.876±0.10	28.6±0.7	-1.777	35.6
2.19	3.966±0.10	28.9±0.7	-1.816	35.5
3.54	3.793±0.10	28.5±0.7	-1.762	35.6
4.75	3.762±0.10	28.4±0.7	-1.883	35.3
5.96	3.971±0.10	28.9±0.7	-2.043	35.0
8.12	3.773±0.10	28.4±0.7	-1.975	35.3
11.39	3.879±0.10	28.7±0.7	-1.366	36.2
14.00	3.894±0.10	28.7±0.7	-0.804	36.4
15.61	4.132±0.10	29.2±0.7	-0.488	36.5
16.57	3.919±0.10	28.7±0.7	-0.535	35.9
16.82	3.707±0.09	28.3±0.7	-0.583	36.1
17.82	3.6267±0.09	28.1±0.7	-0.361	36.3
18.82	3.340±0.08	27.4±0.7	-0.487	36.2
19.57	3.646±0.09	28.3±0.7	-0.440	36.1
20.07	3.443±0.09	27.6±0.7	-0.110	36.8

20.82	3.635±0.09	28.1±0.7	-0.506	36.3
21.57	3.181±0.08	26.9±0.7	-0.230	36.6
22.07	3.259±0.08	27.1±0.7	0.004	36.8
22.70	3.231±0.08	27.1±0.7	-0.158	36.7
23.33	3.370±0.09	27.4±0.7	-0.601	36.0
24.27	3.507±0.09	27.8±0.7	-0.455	36.3
25.22	3.345±0.08	27.4±0.7	-0.525	36.4
25.36	3.183±0.08	26.9±0.7	-0.595	36.2
25.94	3.230±0.08	28.1±0.7	-0.320	36.7
26.51	3.278±0.08	27.2±0.7	-0.437	36.5
27.09	3.434±0.09	27.6±0.7	-0.529	36.2
27.67	3.398±0.09	27.5±0.7	-0.327	36.8
28.22	3.532±0.09	27.8±0.7	-0.518	36.5
28.72	3.703±0.09	28.2±0.7	-0.600	36.2
29.21	3.680±0.09	28.2±0.7	-0.520	36.8
29.70	3.784±0.10	28.4±0.7	-0.732	36.5
30.07	3.610±0.09	28.0±0.7	-0.748	36.5
30.32	3.440±0.09	27.6±0.7	-0.551	36.8
30.57	3.402±0.09	27.5±0.7	-0.617	36.8
30.75	3.331±0.08	27.3±0.7	-0.586	36.9
30.93	3.440±0.09	27.6±0.7	-0.665	36.5
31.11	3.579±0.09	27.9±0.7	-0.559	36.6
31.35	3.423±0.09	27.6±0.7	-0.736	36.5
31.53	3.440±0.09	27.6±0.7	-0.868	36.4
31.65	3.852±0.10	28.6±0.7	-0.646	36.8
31.83	3.456±0.09	27.6±0.7	-0.652	36.7

Bold fonts in age column indicate radiocarbon dated sections.